ORIGINAL ARTICLE

ISAC CYTOMETRY
Journal of Quantitative Cell Science PART A

Collagen Organization Within the Cartilage of *Trpv4*$^{-/-}$ Mice Studied with Two-Photon Microscopy and Polarized Second Harmonic Generation

M. Rocio Servin-Vences,[1†*] Kate Poole,[1‡] Anje Sporbert,[2] Gary R. Lewin,[1] Anca Margineanu[2*]

[1]Molecular Physiology of Somatic Sensation, Max Delbrück Centrum, Berlin, Germany
[2]Advanced Light Microscopy, Max Delbrück Centrum, Berlin, Germany

Received 30 May 2019; Revised 19 July 2019; Accepted 9 September 2019

Grant sponsor: DFG-Gerätezentrum JIMI - joint network for intravital microscopy and imaging, Grant numberNI 1167/3; Grant sponsor: Deutsche Forschungsgemeinschaft, Grant numberSFB958 (A09)

*Correspondence to: Anca Margineanu, Advanced Light Microscopy, Max Delbrück Centrum, Robert Rössle Strasse 10, 13092 Berlin, Germany Email: anca.margineanu@mdc-berlin.de; M. Rocio Servin-Vences, The Scripps Research Institute, 10550 North Torrey Pines Road, La Jolla, CA 92037, Email: rservin@scripps.edu

†Present address: The Scripps Research Institute, La Jolla, California
‡Present address of Kate Poole EMBL Australia Node in Single Molecule Science, School of Medical Sciences, UNSW Sydney, 2052 Sydney, Australia.

Published online 11 October 2019 in Wiley Online Library (wileyonlinelibrary.com)

DOI: 10.1002/cyto.a.23900

© 2019 The Authors. *Cytometry Part A* published by Wiley Periodicals, Inc. on behalf of International Society for Advancement of Cytometry.

This is an open access article under the terms of the Creative Commons Attribution-NonCommercial-NoDerivs License, which permits use and distribution in any medium, provided the original work is properly cited, the use is non-commercial and no modifications or adaptations are made.

Abstract

The polymodal channel TRPV4 has been shown to regulate development and maintenance of cartilage. Here we investigate whether TRPV4 activity regulates the early deposition and structure of collagen matrix in the femoral head cartilage by comparing the 3D morphology and the sub-micrometer organization of the collagen matrix between wild type and *Trpv4*$^{-/-}$ mice pups four to five days old. Two-photon microscopy can be used to conduct label-free imaging of cartilage, as collagen generates a second harmonic signal (second harmonic generation [SHG]) under pulsed infrared excitation. In one set of measurements, we use circularly polarized laser light to reconstruct the 3D morphology of the femoral head cartilage and to measure the tissue thickness. Second, by rotating the direction of the linearly polarized light and using polarized SHG detection, we investigate the sub-micrometer orientation of collagen fibers in the cartilage. At this developmental stage, we cannot detect statistically significant differences between the two mice strains, although a tendency toward a more random orientation of collagen fibers and a higher thickness of the whole cartilage seems to characterize the *Trpv4*$^{-/-}$ mice. We discuss possible reasons for these observations. © 2019 The Authors. *Cytometry Part A* published by Wiley Periodicals, Inc. on behalf of International Society for Advancement of Cytometry.

Key terms

two-photon microscopy; second harmonic generation; polarization microscopy; cartilage; collagen; TRPV4 channels; mechanotransduction

STUDIES of the architecture and function of articular cartilage are particularly important due to the high incidence of pathological conditions such as osteoarthritis (OA), especially in the population > 45 years of age (1). The normal functioning of the articular cartilage is based on an interrelation between (a) the mechanical properties of the cartilage matrix and the articular fluid on the one hand and (b) the anabolic and catabolic processes within the cellular elements (chondrocytes) on the other hand.

The homeostatic maintenance of cartilage depends on the ability of chondrocytes to sense and respond to changing mechanical loads. There are a range of mechanosensors in these cells that have been shown to influence chondrocyte biology, including mechanosensitive ion channels. It has been demonstrated that distinct types of mechanical stimuli can activate different ion channels in primary chondrocytes, where PIEZO1 is activated by cellular compression (2), stretch of the membrane and, to a lesser degree, by tensile inputs applied at the cell–substrate interface (3). In contrast, the polymodal channel TRPV4 is only activated by mechanical inputs that affect the chondrocyte at cell–substrate connections (3).

Manipulation of TRPV4 using pharmacological tools has demonstrated that signaling via TRPV4 can regulate the production of extracellular matrix (ECM) proteins by chondrocytes. In vitro studies using a TRPV4-specific agonist have shown

that TRPV4 activation increases ECM production by chondrocytes even in the absence of a mechanical input (4). In addition, the application of a TRPV4-specific antagonist during cyclic mechanical loading inhibits the mechanically dependent production of matrix (4). What is not clear is how mechanical activation of TRPV4 affects chondrocyte biology and cartilage homeostasis in vivo. This question is particularly difficult to address as TRPV4 has been involved in chondrocyte development (5). In addition, a global knockout of TRPV4 and conditional knockout of TRPV4 in adult chondrocytes have divergent impacts on the development of OA. Namely, *Trpv4*$^{-/-}$ mice are more susceptible to developing age- and obesity-related OA (6), whereas the conditional mutants—where TRPV4 is removed from adult cartilage—are protected against the onset of age-related OA (7). Here we have investigated whether there are structural changes in the cartilage in *Trpv4*$^{-/-}$ mice at an age before the femoral heads have been affected by mechanical loading due to weight bearing and walking, that is, pups 4–5 days old. Given that TRPV4 is mechanically activated by movements of the matrix, by addressing this question, we hope to gain insight into whether matrix production is modulated by TRPV4 during development and early life, when such stimuli are reduced compared with periods of physical activity.

We investigate the morphological characteristics of the femoral head cartilage at the micrometer and sub-micrometer scales using two-photon microscopy in order to understand if the absence of spontaneous and induced Ca^{2+} activation via the TRPV4 channels (2,3,8,9) has consequences on the architecture of the collagen fibers during embryogenesis and fetal development, up to days 4–5 after birth. While cartilage damage during OA progression is typically investigated using radiography and magnetic resonance imaging (10,11), subtle information on the organization of collagen at the molecular and fibrillary levels can be obtained using microscopy techniques. Electron microscopy and small-angle X-ray diffraction have been utilized in literature to study the structure and orientation of collagen fibers at the nanometer scale (12,13), but the drawback of these techniques is that they provide only a snapshot on a relatively small scale of the whole sample. Staining of tissue sections or cellular assemblies using picrosirius red enables visualization of collagen fiber distribution in light microscopy on the micrometer scale, and sample observation between cross-polarizers can reveal information also on the sub-micrometer alignment of collagen fibers (14). On a larger scale, optical coherent tomography (OCT) and polarization-sensitive OCT have also been used, but these techniques suffer from averaging over a larger volume due to their low axial resolution, in the order of tens of micrometers (15,16).

The property of collagen to generate second harmonic signal (second harmonic generation [SHG]) when excited in two-photon microscopy has been applied to study native collagen in tissues, as it provides a label-free imaging method while preserving the sub-micrometer resolution of confocal microscopy. The SHG is the property of non-centrosymmetric molecules or supramolecular assemblies (i.e., molecules or assemblies without a symmetry center) to scatter an incident radiation at half the excitation wavelength. This condition is met in biology by helical molecules such as collagen and its supramolecular fibrillary assemblies. Collagen type I organization is the most studied using this method, as it provides a high SHG signal due to the formation of long and thick bundles (30–500 nm in diameter, up to 1 cm length), for example in skin, tendons, ligaments, organ capsules, or connective tissue (17). Collagen type II, which is found in the cartilage, forms much smaller and thinner fibrils, with a diameter of ~48 nm due to the interposition of collagen IX (12), giving a lower SHG signal, and therefore harder to detect.

Adding polarized excitation and detection in all light microscopy techniques (including two-photon microscopy) confers a supplementary dimension to the images (in addition to intensity) by giving information on the molecular orientation (18,19). As shown in Figure 1A, the laser linearly polarized in the *xy* plane excites the collagen fibers (represented as a triple helix) with a given 3D orientation. The fibers are preferentially excited if their long axis is aligned along the laser polarization direction. The intensity of the emitted SHG signal is proportional to the magnitude of the fiber projections on the *x*- and *y*-axes (which depend, on their turn, on the angles formed by the fiber with the three axes—*x*, *y*, and *z*). Note that the signal emitted in the *z* direction cannot be measured in this configuration and requires other experimental setups for detection (20).

Materials and Methods

Sample Preparation

Femoral bones with cartilage topping the head have been obtained from pups aged 4–5 days. Two mouse strains have been used in this study: the wild type (WT) C57Bl/6 from Charles River (Wilmington, MA) and the knockout strain lacking the expression of the mechanosensitive voltage channel Trpv4 (*Trpv4*$^{-/-}$, Jackson Laboratory (Bar Harbor, ME), MGI ID: 2667379 on a C57Bl/6 background) (21). The dissected femoral heads were washed with phosphate buffer saline (PBS), then immediately immersed in 80% glycerol, and frozen in liquid nitrogen. All samples have been imaged within 2 weeks after the collection. On the day of the experiment, the samples were thawed on ice and washed with PBS to remove the excess of glycerol, then mounted in 1% low-melting point agarose, and covered with a cover glass no. 1.5 for imaging. The femoral heads were placed with the intra-articular ligament facing upward (as shown in Fig. 1C), trying to ensure that all samples were fixed in the same orientation. All animal works have been done in compliance with protocols approved by the German Federal authorities (State of Berlin).

Two-Photon Microscopy

SHG images have been acquired with a two-photon microscope (Trimscope I; LaVision Biotec GmbH, Bielefeld, Germany) custom modified for polarization measurements

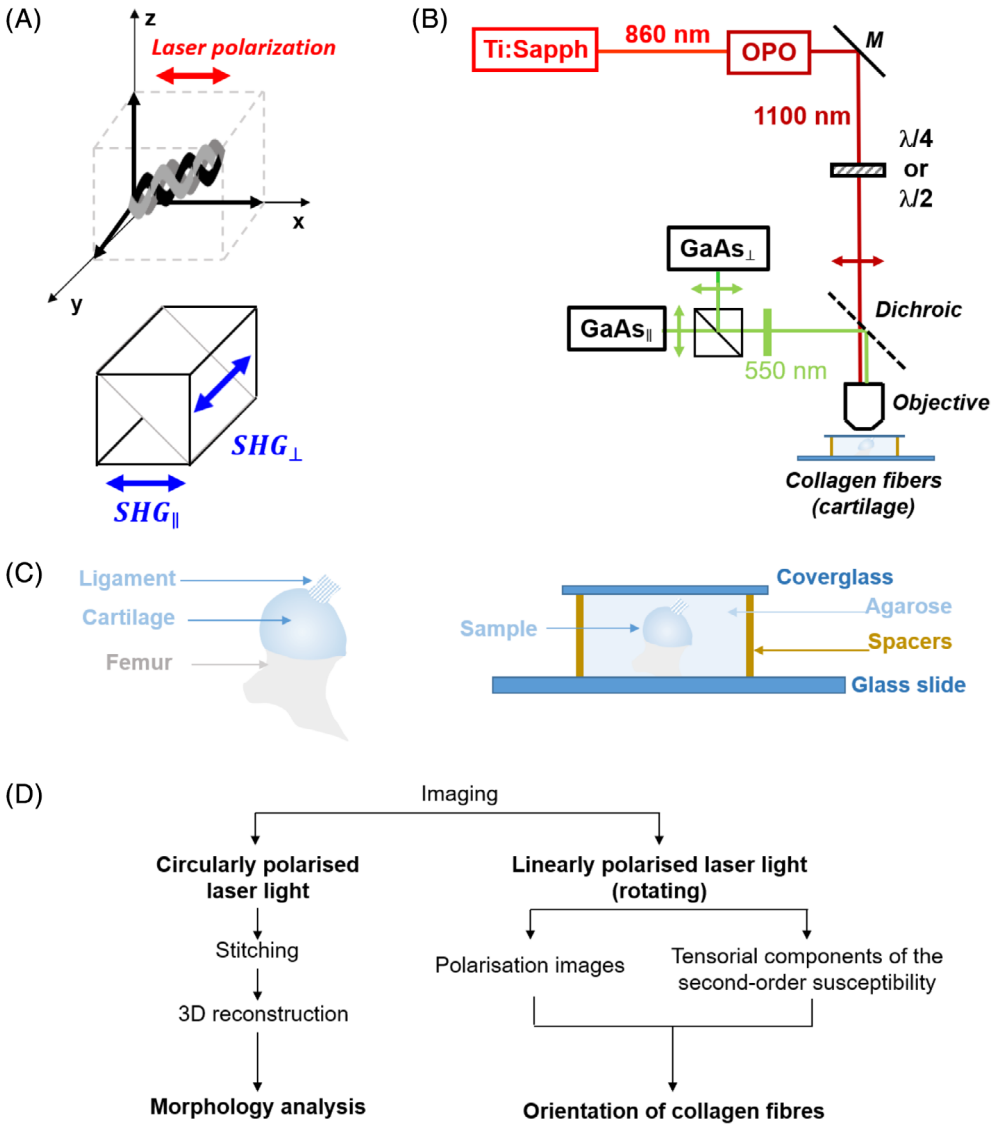

Figure 1. (**A**) Schematic of collagen fiber excitation and SHG detection in a polarization experiment. Collagen is represented as a triple helix with a 3D orientation. When the linearly polarized laser excites the fiber, the intensity of the SHG signal detected on the parallel or perpendicular direction relative to the laser depends on the magnitude of the fiber projections along the *x*- and *y*-axes. (**B**) Schematic of the two-photon setup for polarized SHG measurements of the cartilage. (**C**) Schematic of the femoral head and of the sample preparation for imaging. (**D**) Workflow of image acquisition and analysis to obtain information on morphology and orientation of collagen fibers within the cartilage. [Color figure can be viewed at wileyonlinelibrary.com]

(Fig. 1B). The SHG signal of the femoral cartilage was generated using 1,100 nm excitation wavelength from an optical parametric oscillator (OPO) (APE, Berlin, Germany) pumped by a Titanium:Sapphire laser (Chameleon Ultra II; Coherent, Santa Clara, CA). The OPO wavelength was chosen to avoid the Titanium:Sapphire path, which contains other polarization-active elements. The OPO beam was passed through a polarizing beam splitter (Thorlabs, Newton, NJ) to clean up the polarization direction and then either through a quarter-wave plate (Thorlabs) to obtain circularly polarized light or through a half-wave plate (Thorlabs) to rotate the plane of the linearly polarized light. Rotation of the polarization plane of the OPO beam was achieved by placing the half-wave plate in a motorized rotation mount (Thorlabs). Thus, the collagen fibers of the cartilage with different orientations could be sequentially excited. A water immersion Olympus 20×, 0.9 NA, objective dedicated for multiphoton excitation was used for imaging. The SHG signal was detected in the backward direction using a 560/40 nm emission filter. The emitted light was then split using a polarizing beam splitter (Thorlabs) between two GaAs detectors (LaVision Biotec GmbH).

Using circularly polarized excitation, the whole cartilage structure was scanned using 3 × 3 tiles (400 × 400 μm each) and a depth of ~500 μm. The tiles were stitched in ImageJ/Fiji (22). The merged SHG intensities measured in the parallel and perpendicular channels using circularly polarized light were used to reconstruct the 3D structure of the whole cartilage in Imaris (Bitplane/Andor, Belfast, UK). All other image processing was done in ImageJ/Fiji (https://fiji.sc/).

Using linearly polarized excitation, only one confocal plane (400 × 400 μm, 512 × 512 pixels) was selected and imaged using different rotation angles of the half-wave plate. The plane was chosen close to the top of the cartilage structure, avoiding the ligament region.

To correct for the different transmission and collection efficiencies of the system for the parallel and perpendicular directions, a rhodamine 6G solution in water (with very fast depolarization time) was measured for every experiment using both circularly and linearly polarized excitation. The correction factor G was calculated:

$$G = \frac{I_{\perp \mathrm{Rh6G}}}{I_{\parallel \mathrm{Rh6G}}} \quad (1)$$

where $I_{\parallel Rh6G}$ and $I_{\perp Rh6G}$ are the intensities measured for the rhodamine 6G solution in the parallel and perpendicular channels, respectively.

The SHG intensity images of the cartilage in the parallel and perpendicular channels were also corrected by background subtraction.

Polarization images of the SHG signal were calculated using the formula:

$$p = \frac{I_{\parallel} - GI_{\perp}}{I_{\parallel} + GI_{\perp}} \quad (2)$$

The parallel detection channel was considered for all images relative to the 0° orientation of the half-wave plate.

Histograms of polarization values per pixel were obtained in ImageJ/Fiji, and further statistical analysis was done in the open source software R (https://www.r-project.org/) using the fitdistrplus package (23). The background contribution to the histogram of polarization values has been excluded by creating a mask from the intensity images after applying a band-pass fast Fourier transform (FFT) filter.

The SHG intensity images obtained along the parallel direction using linearly polarized light were plotted against the rotation angle of the half-wave plate, and the curve was fitted with a model from literature (24) using the Matlab software (Mathworks, 2018, Natick, MA):

$$I_{\parallel} = A\cos 4\alpha + B\cos 2\alpha + C \quad (3)$$

where $I_{\parallel}$ is the SHG intensity measured along the parallel direction, α is the rotation angle of the polarization direction, and A, B, and C are fitting parameters that can be further used to calculate the ratio ρ of the two independent tensorial components of the second-order susceptibility (χ_{xxx}, χ_{xyy}) (see Ref. 24 for notation details):

$$\rho = \frac{\chi_{xxx}}{\chi_{xyy}} \quad (4)$$

$$\rho^2 = \frac{A + B + C}{A - B + C} \quad (5)$$

Graphs were plotted in Matlab or GraphPad Prism (GraphPad, San Diego, CA).

Results

To investigate the collagen structure in articular cartilage, we obtained images of samples from 4–5-day-old mice pups, six WT mice, and seven *Trpv4*$^{-/-}$ mice. All average and standard deviation values are reported on these number of samples (n = 6 for WT and n = 7 for *Trpv4*$^{-/-}$).

The femoral heads with a layer of intact cartilage were immobilized in low-melting-point agarose with the intra-articular ligament facing upward to ensure that the surface of the cartilage was imaged with the highest resolution of the microscope, corresponding to the *xy* plane (Fig. 1C).

In a standard configuration, the SHG of collagen fibers aligned parallel with the polarization direction of the illuminating two-photon laser will be preferentially excited. In order to circumvent this limitation, we modified the excitation path in two ways (Fig. 1B):

a. By inserting a quarter-wave plate (λ/4), circularly polarized light was obtained, to equally excite the collagen fibers in all directions in the *xy* plane of the microscope.
b. By inserting a half-wave plate with the possibility of rotation, images were acquired at multiple excitation angles, from 0° to 180° in steps of 10°.

We additionally modified the detection path of the microscope by inserting a polarizer between two sensitive GaAs detectors, allowing the acquisition of the SHG images on a parallel and a perpendicular direction relative to the laser polarization direction.

In order to obtain morphological information on the femoral cartilage structure, we acquired SHG intensity images with circularly polarized light excitation. To extract information on the orientation of collagen fibers within the cartilage, we used the parallel and perpendicular images obtained with linearly polarized light excitation (Fig. 1D).

Morphology Analysis of the 3D Cartilage Structure

Using the circularly polarized light, the whole femoral head structure was scanned in *xyz* using 3 × 3 tiles that were stitched and rendered in 3D. Figure 2 shows an example of such 3D reconstruction, where the cartilage network generating the SHG signal is visible and delineates the lacunae holding the chondrocytes. The cellular structures are not visible, as they do not generate SHG signal. The overall morphology

of the femoral cartilage is very similar for the WT and *Trpv4*$^{-/-}$ samples.

To analyze the thickness of the cartilage, we measured transversal sections at different depths: 200, 300, and 400 μm below the end of the ligament (Fig. 3A). On these sections, the femoral head cartilage appears as a ring-shaped structure (Fig. 3B). The Radial Profile plugin implemented in ImageJ/Fiji (https://imagej.nih.gov/ij/plugins/radial-profile.html) was then used to quantitate the integrated intensity as a function of distance from the center of a circle defined around the cartilage structure (Fig. 3B, yellow circle). The resulting plots were normalized according to the highest intensity value (Fig. 3C). To estimate the width of the cartilage, we applied two approaches. First, the widths at 25%, 50%, and 75% from the normalized peak intensity were measured (Fig. 3C). Second, the integrated area under the curve was also calculated. Although the average values of all these measurements indicate that the cartilage of the *Trpv4*$^{-/-}$ mice has a tendency toward increased thickness, no statistically significant differences were detected between any of these parameters (Fig. 3D,E).

Analysis of Collagen Fiber Orientation from Polarization Images

We then investigated whether there were changes in the orientation of collagen fibers in articular cartilage isolated from the *Trpv4*$^{-/-}$ mice. Images were acquired with linearly polarized laser excitation, and emission was split between two detectors using a polarizing cube. Figure 4A explains how these images provide information on the orientation of the collagen fibers. The linearly polarized laser light preferentially excites the collagen fibers parallel with the polarization direction. If these fibers are also oriented along the parallel direction of the polarizing cube, the intensity along this direction will exhibit a higher intensity. The fibers oriented at an angle relative to the laser polarization direction will emit on either the parallel or the perpendicular channel, depending on the angle: the higher this angle, the more light will be emitted on the perpendicular direction of the polarizing cube. Fibers with 90° orientation relative to the laser excitation direction will not be excited and thus not contribute to the images. When the laser polarization direction rotates, different collagen fibers within the composition of the cartilage will be excited and will emit either on the parallel or the perpendicular direction of the cube, depending on their orientation. Thus, the SHG intensity varies along the parallel and the perpendicular directions with the rotation of the polarization direction of the laser, as shown in Figure 4B. Using these intensity values, the polarization parameter $p = \frac{I_{\parallel} - GI_{\perp}}{I_{\parallel} + GI_{\perp}}$ can be calculated (see also Materials and Methods for the explanation of G). The

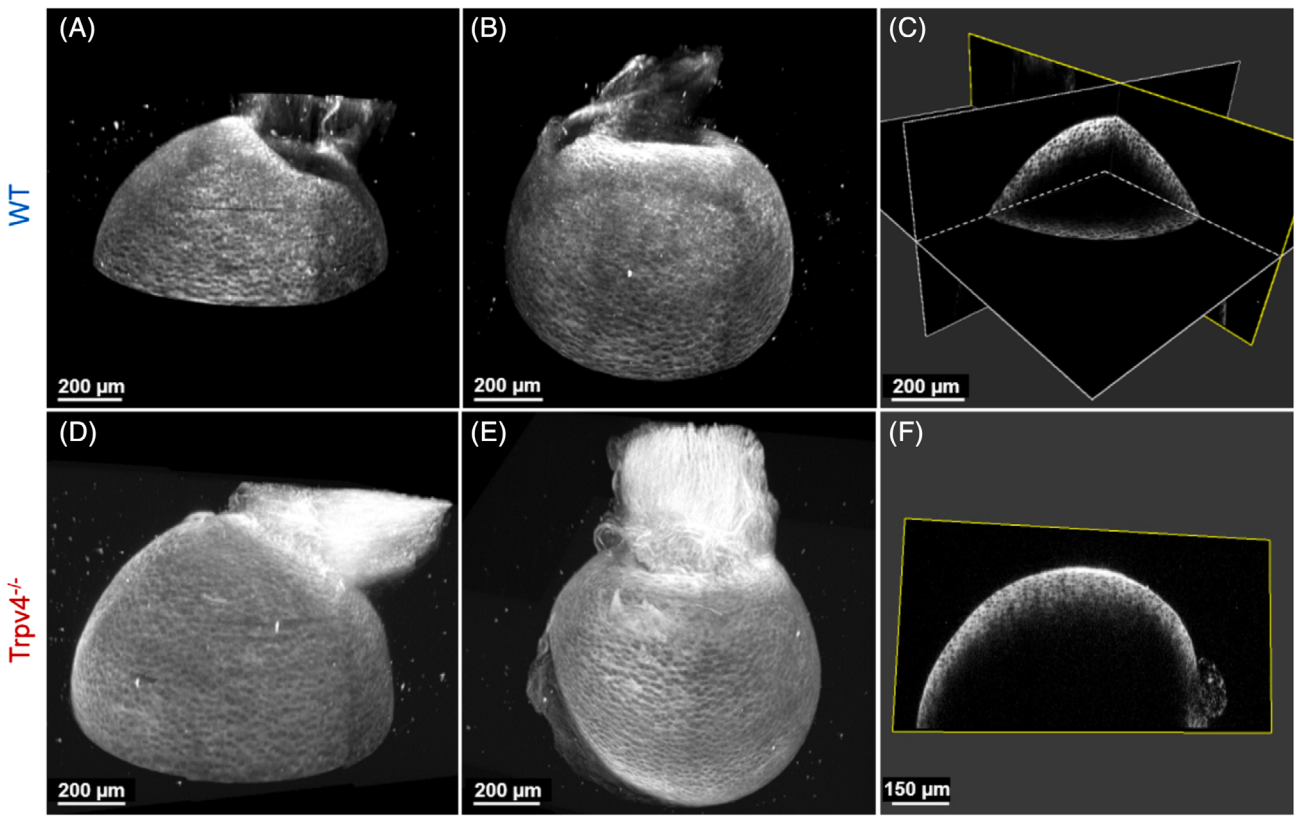

Figure 2. 3D reconstruction of the mouse femoral head cartilage and ligament using the merged SHG intensity in the parallel and perpendicular channels. Top row: lateral view (**A**), top view (**B**), and a cross section along three perpendicular planes through the cartilage (**C**) for a WT sample. Bottom row: lateral view (**D**), top view (**E**), and a sagittal cross section (**F**) on one of the *Trpv4*$^{-/-}$ samples. [Color figure can be viewed at wileyonlinelibrary.com]

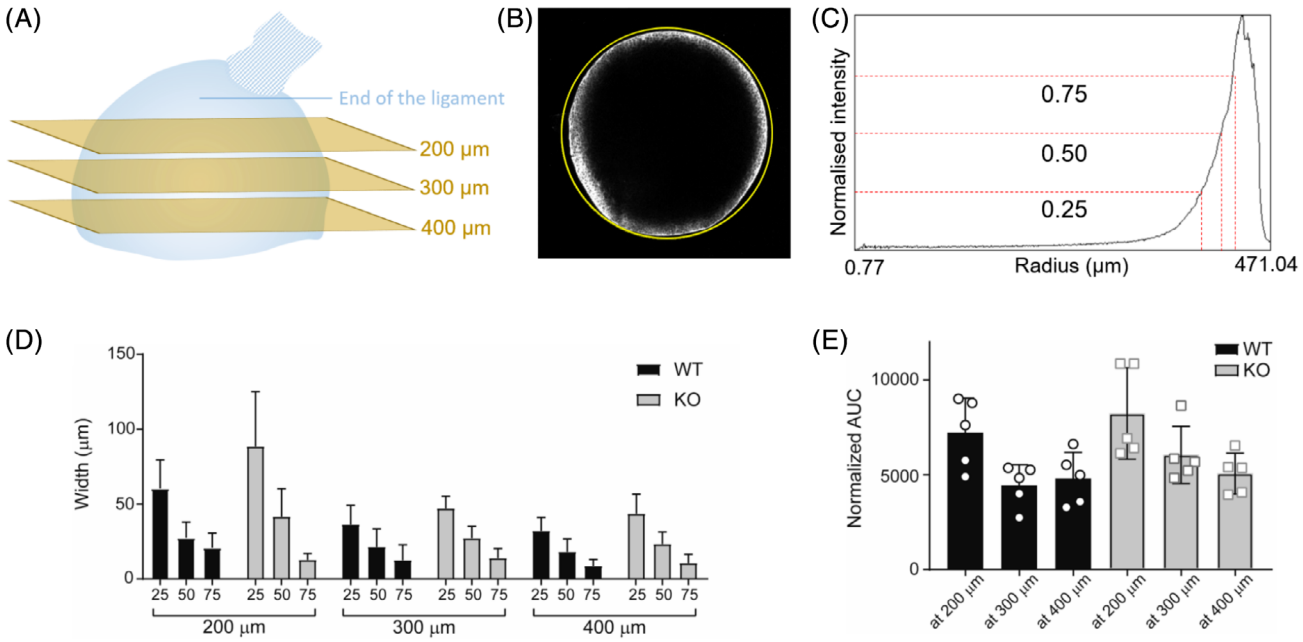

Figure 3. Morphological analysis of cartilage SHG images. (**A**) Schematic of the femoral head cartilage and of the intra-articular ligament. On the 3D reconstructed image, transversal planes were selected at 200, 300, and 400 µm below the end of the ligament. (**B**) Example of a transversal section on the 3D structure shows a ring pattern, with the highest SHG signal at the periphery. When using the Radial Profile plugin implemented in ImageJ/Fiji, a circle (yellow) is generated and its size can be adjusted to cover the entire transversal tissue section. (**C**) The Radial Profile analysis results in a plot with integrated intensities as a function of distance from the center of the circle. On the normalized plot, the width of the peak (black solid line) was measured at 75%, 50%, and 25% from the maximum intensity (red dashed lines). (**D**) Statistical analysis of the widths of femoral head cartilages measured at 200, 300, and 400 µm and at 25%, 50%, and 75% from the maximum intensity peak. Mean values and standard deviations are plotted: WT (black) and the *Trpv4*$^{-/-}$ (gray) samples. (**E**) Statistical analysis of the area under the curve (AUC) calculated on the intensity radial profiles plot. Mean values and standard deviations are plotted: WT (black) and *Trpv4*$^{-/-}$ (gray) mice. The round and square symbols indicate the normalized values per femoral head that was imaged. [Color figure can be viewed at wileyonlinelibrary.com]

parameter p also shows variations with the orientation angles of the laser polarization direction (Fig. 4C). As the SHG emitted along the perpendicular direction can have higher values for some orientation angles of the laser excitation direction, p can take negative values.

Polarization images were calculated on a pixel-by-pixel basis for all WT and *Trpv4*$^{-/-}$ cartilage samples (Fig. 4D) and statistically analyzed (Fig. 5). Example histograms of polarization values p for individual images measured for WT and *Trpv4*$^{-/-}$mice are shown in Figure 5A. The total histograms of these values have been obtained by putting together the values in all pixels of the polarization images obtained at all laser excitation angles (Fig. 5B). These data indicate that the polarization parameter tends to be distributed toward higher values for the WT samples compared with the *Trpv4*$^{-/-}$ samples. Interestingly, the amplitudes of the two peaks of the histogram are similar in the distribution calculated for the WT samples, while the amplitude of the peak situated at negative (i.e., low) polarization values is higher for the *Trpv4*$^{-/-}$ samples. Higher polarization values (p) come from a higher intensity of the SHG signal detected along the parallel direction of the polarizing cube splitter. Thus, these results show that the WT cartilage tends to have more collagen fibers aligned with the parallel direction of the detection. In the *Trpv4*$^{-/-}$ samples, the fibers seem to be more randomly oriented along multiple directions, as the intensity emitted along the perpendicular direction is higher.

The total histograms of polarization values have a complex shape, and therefore, it is difficult to find a model to fit them. To understand better where differences between the two groups of samples occur, we analyzed individual histograms obtained at each rotation angle of the laser excitation direction. We observed that the distribution of p values in individual histograms is not always symmetric; so we analyzed the skewness of these distributions. This parameter indicates how well the histogram resembles a normal (Gaussian) distribution. A skewness value around 0 indicates a symmetric Gaussian distribution, while positive or negative skewness values indicate that the distribution is not symmetric, with tails observed toward positive or negative values. Depending on the incidence angle of the laser, the distributions of the polarization values for both types of samples were either normal or nonsymmetric (Fig. 5C). Therefore, we considered the median and the interquartile range rather than mean and standard deviation to compare these distributions. At all rotation angles, a tendency toward lower median polarization values is observed for the *Trpv4*$^{-/-}$ mutants compared with the WT mice (Fig. 5D), similar to the total histogram.

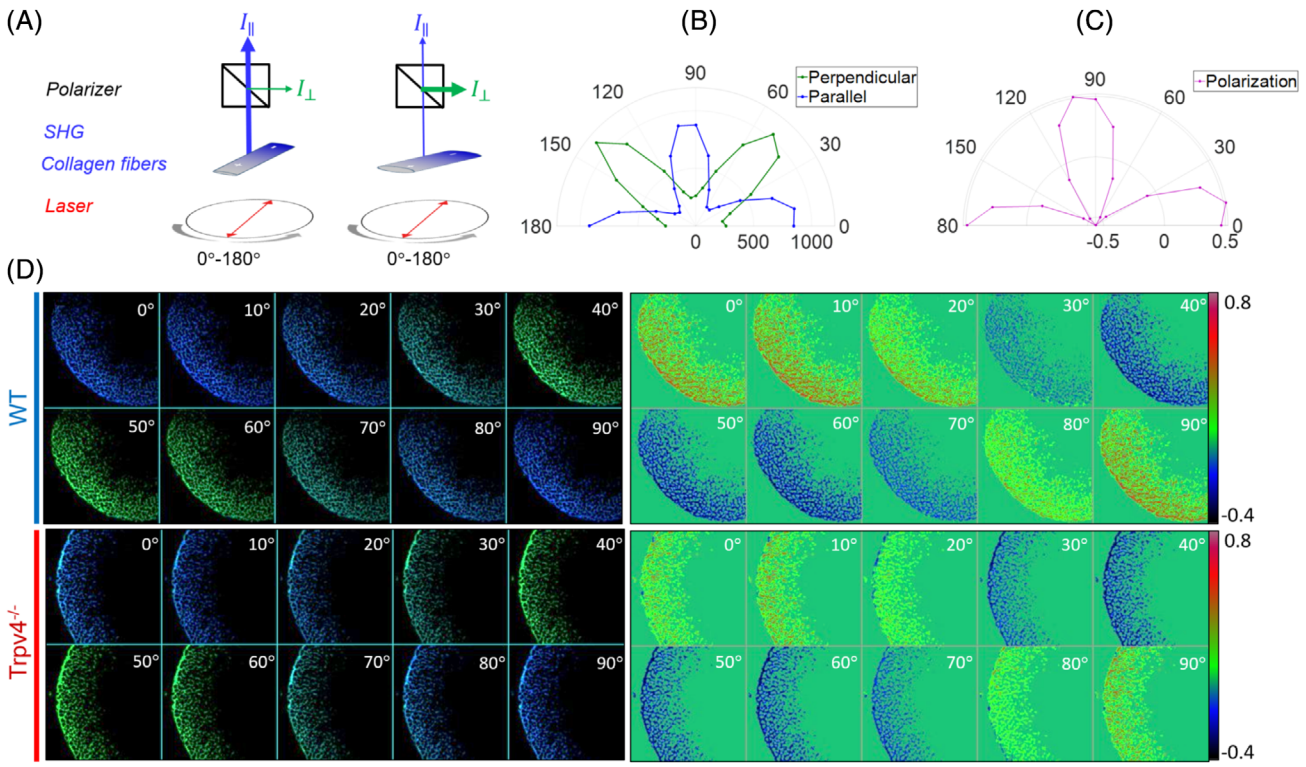

Figure 4. (**A**) Schematic of the polarization image acquisition. (**B**) Example of SHG intensities measured along the parallel and the perpendicular directions when the polarization direction of the laser is rotated between 0° and 180° (the angles correspond to the orientation of the λ/2 plate). (**C**) Example of polarization values *p* calculated from the SHG intensities measured along the parallel and the perpendicular directions when the polarization direction of the laser is rotated between 0° and 180°. (**D**) Representative images of the SHG intensities acquired along the parallel (blue) and the perpendicular (green) directions when the polarization direction of the laser is rotated between 0° and 90°. The two upper rows correspond to a sample obtained from a WT mouse, and the two lower rows are images of a sample obtained from *Trpv4*$^{-/-}$ mice. The corresponding color-coded polarization images are shown on the right-hand side. [Color figure can be viewed at wileyonlinelibrary.com]

The spread of the values within individual histograms is indicated by the interquartile range. For most of the rotation angles, the mutant samples show slightly higher interquartile ranges, that is, slightly higher spread of the polarization values (Fig. 5E). We interpret the tendency toward higher spread of the *p* values in the mutant samples (indicated by the interquartile range and skewness) as a tendency toward a more random orientation of the collagen fibers in mutants compared with the WT samples.

Although all the parameters measured for the distribution of the polarization values indicate a tendency toward a higher spread of the orientation of the collagen fibers in *Trpv4*$^{-/-}$ samples, we could not conclude that there is a statistically significant difference between the mutants and the WT mice within the error limits given by the standard deviation (plotted on Fig. 5C,D,E).

Analysis of Collagen Fiber Orientation from SHG Intensity Images

We next applied a second approach to ask if the orientation of collagen fibers in articular cartilage differs in *Trpv4*$^{-/-}$ samples. Under the influence of the oscillating light electric field, separation of molecular charges occurs in the collagen fibrillary structures (Fig. 6A). The magnitude of the charge separation has a nonlinear dependence on the laser intensity in two-photon microscopy, when high power, pulsed laser sources are used (for a review, see Ref. (25)). This property is known as second-order polarizability (or susceptibility). Furthermore, due to the elongated form of the collagen fibers, the amplitude of the charge separation is not the same on all spatial directions (Fig. 6A). This is mathematically described using a 3D vector (or tensor), which takes into account both the magnitude and orientation of the generated electrical fields in the fibers, as well as the direction of the laser in 3D. Thus, by evaluating the ratio between the tensorial components of the second-order susceptibility along the long and short axis of collagen fibers, it is possible to obtain information on the orientation of the collagen fibers. This can be done by fitting appropriate equations to the SHG intensity images obtained via the rotation of the direction of the laser polarization. Analytical expressions have been derived for both the case when the total SHG intensity is measured (26), as well as when the SHG intensity is detected along the parallel and perpendicular directions (24). We have used the second approach and fitted the SHG intensity along the parallel direction of detection using Eq. 3 (Materials and Methods).

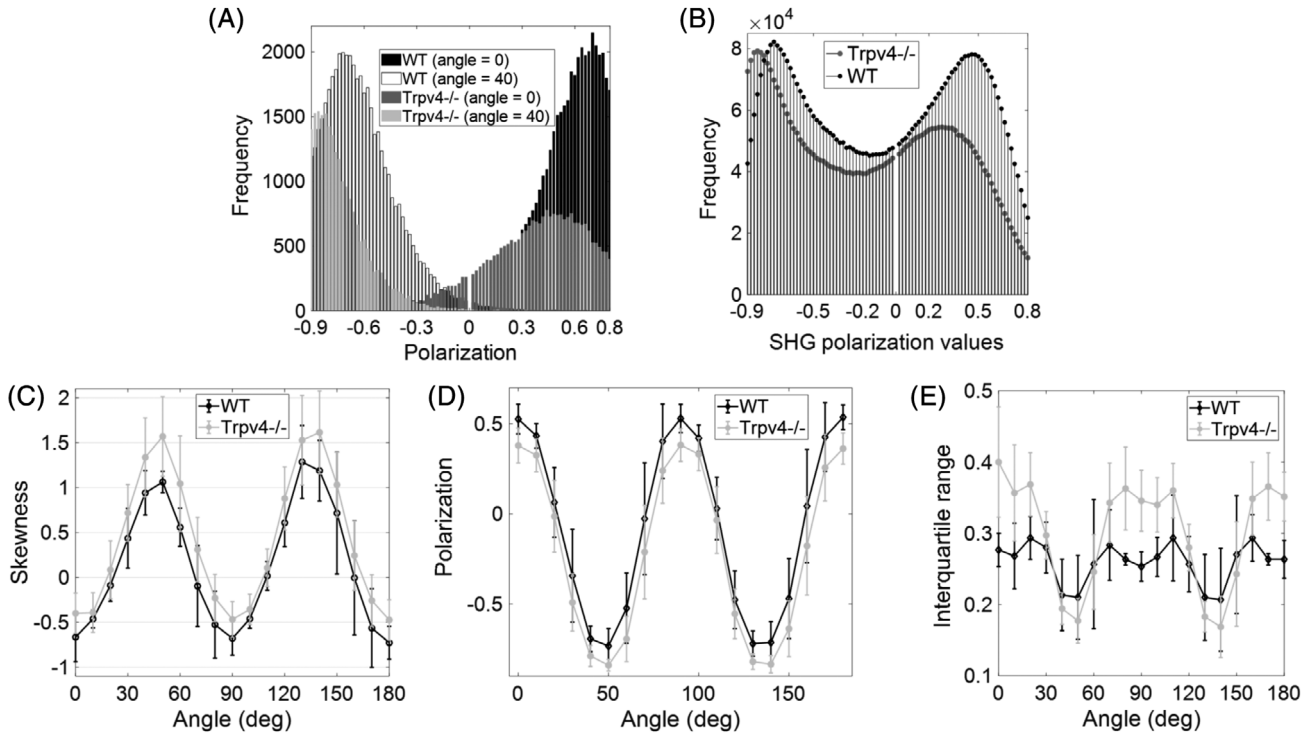

Figure 5. Statistical analysis of the SHG polarization images. (**A**) Examples of histograms of pixel polarization values for WT (black and white *bars*) and knockout (*gray*) at two different angles of the laser rotation. The 0 value of polarization has been excluded from the histograms, as most pixels with this value belong to the background, after masking the images. (**B**) Total histograms of the polarization values on images obtained at all laser rotation angles. (**C**) Skewness of the polarization value distributions calculated at all measured angles. (**D**) Median polarization values calculated for individual histograms at different angles. (**E**) Interquartile range of the polarization value distributions calculated at all measured angles. On all graphs, gray lines and markers indicate *Trpv4*$^{-/-}$ samples and black WT samples.

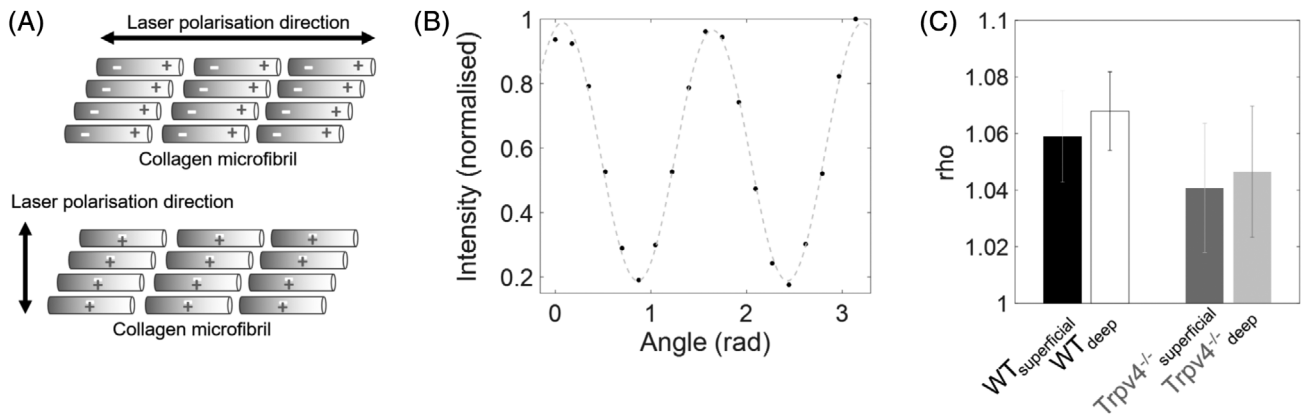

Figure 6. (**A**) Schematic of the charge separation in collagen fibers depending on the orientation direction of the two-photon laser excitation. (**B**) The values of the SHG signal emitted along the parallel direction (black dots) of detection were fitted with Eq. 3 (Materials and Methods) (gray dotted line). (**C**) The average ratios of two independent tensorial components of the second-order susceptibility of collagen fibers and their standard deviations (SD).

An example of such fit on a *Trpv4*$^{-/-}$ sample is shown in Figure 6B. The average ratios of two tensorial components of the second-order susceptibility of collagen fibers (Eq. 4 and 5 in *Materials and Methods*) and their standard deviations calculated for the WT and mutant samples are shown in Figure 6C. Fitting was done separately on the integrated intensity in the most superficial layer (~20 μm from the cartilage surface) and the integrated intensity across the rest of the cartilage on each image. No significant differences could be observed between the superficial and the deeper zones for

either WT or mutant samples using the integrated intensity values (Fig. 6C). The average value of the two tensorial component ratio is closer to 1 in the case of *Trpv4*$^{-/-}$ mice, possibly indicating again the tendency of collagen fibers to be more randomly oriented in different directions. However, also from this analysis, we cannot conclude a statistically significant difference between the two groups.

Discussion

In previous studies, we have focused on the influence of the ECM on the function of the mechanosensitive channels (3). In this study, we aimed to explore the inverse relationship and to see if we can identify possible correlations between the expression of the TRPV4 channel and the organization of the collagen fibers forming the cartilage. We addressed this question in an animal model rather than isolated cells. Our model was chosen based on the observation that the *Trpv4*$^{-/-}$ mice are known to develop OA (6,27), thus alterations in the cartilage structure, in contrast to the conditional deletion in adult mice which was shown to protect against OA development (7). However, in human patients, mutations in the TRPV4 gene can lead to joint dysfunction (28,29), with joint defects exacerbated in load-bearing regions. These data highlight the fact that TRPV4 can have variable impacts depending on when the channel is ablated, and these differences may reflect diversity in activation via mechanical inputs. The impact of TRPV4 signaling is further complicated by the fact that TRPV4 has been implicated in chondrogenic differentiation (5). In addition, TRPV4 inactivation disrupts collagen deposition in mesenchymal stem cells (30). These data suggest that TRPV4 may be required for ECM deposition during the development of the cartilage tissue.

In order to determine whether cartilage is malformed when TRPV4 is absent during development, our study was conducted using a label-free imaging technique based on the measurement of the SHG signal under two-photon excitation. The structure of the osteoarthritic cartilage has been investigated before using SHG, but data were obtained on cartilage samples subjected to mechanical load, either after surgical induction of OA in mice (31–33) or from patients undergoing knee surgery for OA (34–36). Our present contribution aims to correlate the structural modifications of the cartilage matrix with molecular mechanisms affecting the chondrocytes (i.e., reduction of Ca^{2+} transients due to the absence of the TRPV4 channels) at a time point post-cartilage development but before the tissue has been subjected to ongoing mechanical loads, that is, in pups at P4–5. In addition, at this developmental stage, the cartilage is known to be thicker than at adult stages (37), and the bone ossification process is not yet fully finished, thus avoiding the overwhelming contribution of bone SHG signals to the imaging (32). We compared features within the whole structure of the femoral cartilage, as well as the sub-micrometer scale orientation of collagen microfibrils in the femoral cartilage of the two groups of mice.

The overall morphological structure of the femoral cartilage was imaged with circularly polarized light to excite with equal probability fibers oriented in different directions of the space. Quantitative measurements of the cartilage thickness did not demonstrate statistically significant differences between WT and *Trpv4*$^{-/-}$ mice, although a tendency toward higher mean values of the thickness was observed for the mutant samples (Fig. 3D,E). This observation could be correlated with other results obtained at the cellular level, showing the requirement of active TRPV4 channels for collagen compaction (38).

The orientation of collagen fibers was explored at the sub-micrometer scale by exciting the samples with linearly polarized laser light and detecting the emission of the SHG signal with two detectors, aligned parallel and perpendicular to the excitation direction. Rotating the direction of the laser light ensures the sequential excitation of fibers with all spatial orientations in the *xy* plane. However, this does not explore molecular orientations along the *z*-axis. The calculated polarization parameter p offers information on the ratio between the light detected along the parallel and the perpendicular directions. Lower values of p for the same orientation of the laser excitation imply more collagen fibers emitting along the perpendicular direction of detection. A tendency toward lower p values has been observed for mutant samples and might indicate that the collagen fibers have more scattered orientations along different spatial directions compared with the WT mice (Fig. 5) at 5 days old. However, the detailed statistical analysis did not reveal significant differences between the two groups. This tendency to a more random orientation of collagen fibers in *Trpv4*$^{-/-}$ mice is also supported by the lower values of the ratio of two tensorial components of the second-order susceptibility of collagen fibers, but again, without showing significant differences with the WT group (Fig. 6). The trend of a more disorganized collagen II matrix in *Trpv4*$^{-/-}$ mice suggests that over time (aging) and extra load (overweight), the cartilage could be more prone to develop OA, as observed before (6,27).

Although our measurements point toward more scattered orientations of collagen fibers in *Trpv4*$^{-/-}$ mice, the differences were not statistically significant compared with WT samples at this age (4–5 days after birth). We interpret these data in the view of some recent results obtained by Gilchrist et al. (30). Using stem mesenchymal cells grown on micropatterned substrates, the authors demonstrate that continuous exposure to TRPV4 channel inhibitors leads to a marked decrease in the deposition of aligned collagen fibers after 14 days in 2D substrates. However, the cell signaling (measured by quantitation of Ca^{2+} spontaneous oscillations) decreases significantly during the first day and recovers back to control levels after 7 days in the continuous presence of TRPV4 channel inhibitors. This means that adaptive mechanisms are in place to compensate for reduced Ca^{2+} signaling via TRPV4 channels, which might also be the case in the embryonic cartilage. This hypothesis is supported by our recent data analyzing the activation of mechanosensitive channels in primary chondrocytes. We noted that in WT

cells, the application of a TRPV4-specific antagonist reduced mechanically activated currents to 13 ± 6% or the original magnitude. In contrast, in cells isolated from a *Trpv4*$^{-/-}$ mouse, mechanosensitive channel activity was only reduced to around 50%, indicating a compensatory current was present when TRPV4 was chronically ablated. Knockdown of PIEZO1 transcripts in the *Trpv4*$^{-/-}$ cells completely ablated the currents, suggesting that PIEZO1 can compensate for a chronic loss of TRPV4 (3,39). In addition, the cartilage is a complex environment where collagen II fibers associate with proteoglycans and other collagens to stabilize the network (40). Thus, the additional ECM proteins might have an influence on collagen II deposition and alignment in a 3D environment. One important difference between animal samples and isolated cells is that collagen deposition still occurs in the *Trpv4*$^{-/-}$ mouse cartilage during the intrauterine development and the first few days after birth at comparable levels with the WT mice. We propose that significant differences with the WT mice could not be observed in the orientation of collagen fibers because at this stage of development, the mechanical load on the articular cartilage is minimal and compensatory mechanisms take place. Indeed, substantial modifications of the structure of the osteoarthritic cartilage have been observed 8 weeks after the surgical induction of OA in mice (31,32) or in human samples where the advanced stage of OA progression required surgical replacement of the joint (34–36).

It is also possible that in our measurements, the differences are somehow mitigated by the lack of very precise alignment of the cartilage supported by the femoral bone along the *z*-axis. Sample fixation in agarose was done manually, and although we tried to keep the ligament upward, small variations in the angle were possible. This could influence the magnitude of the *xy* projections both for measuring the cartilage thickness on the 3D reconstructed images and for estimating the polarization values.

Using 1,100 nm wavelength and a 0.9 NA objective, we excite fibers in a confocal volume of ~730 nm in the *xy* and > 2 μm in the *z* directions. Given the small thickness of collagen II fibers (~50 nm), we probably average over a relatively high number of fibers, with possible different orientations. Furthermore, it was shown that with high NA excitation, collagen fibers with an off-plane tilt above 50° could introduce extra polarization coupling contributions from out-of-plane components (36), influencing the *p* values in the *xy* plane.

The initial experiments presented here demonstrate that the impact of a loss of TRPV4 on cartilage biology is likely not due to malformation of the cartilage but due to a slower process that occurs over time. Future studies are necessary to investigate the progression of fiber alignment at later stages in the development, after the articular cartilage has been submitted to physiological mechanical load. To the best of our knowledge, an intravital examination of the osteoarthritic cartilage using two-photon microscopy and SHG has not yet been published. Understanding the different stages of the disease progression requires finding new techniques for longitudinal intravital imaging of the articular cartilage. These regions are not easily accessible with microscope objectives, but recent developments of GRIN lenses for the exploration of deep organs and cavities in live animals (41,42), as well as the first report on preclinical translation of SHG microscopy to the meniscal and articular cartilage (43), could provide solutions for this problem.

Acknowledgments

This project was partly supported via the Deutsche Forschungsgemeinschaft (DFG) grant SFB958 (Project A09 to K.P. and G.R.L.). Funding for the custom implementation of the polarization components in the two-photon setup was obtained via the Deutsche Forschungsgemeinschaft (DFG) grant NI 1167/3 DFG-Gerätezentrum JIMI—Joint Network for Intravital Microscopy and Imaging. We acknowledge the contribution of Dr. Raluca Niesner and Dr. Anja Hauser for their participation to this grant. K.P. thanks to the Cécile Vogt fellowship awarded by Max Delbrück Center for Molecular Medicine in the Helmholz Association. The general maintenance of the setup is supported via funding from the Max Delbrück Center for Molecular Medicine in the Helmholz Association and by the staff of the Advanced Light Microscopy.

Conflict of Interest

Authors declare no conflict of interest.

Literature Cited

1. Zhang Y, Jordan JM. Epidemiology of osteoarthritis. Clin Geriatr Med 2010;26(3):355–369. https://doi.org/10.1016/j.cger.2010.03.001.
2. Lee W, Leddy HA, Chen Y, Lee SH, Zelenski NA, McNulty AL, Wu J, Beicker KN, Coles J, Zauscher S, et al. Synergy between Piezo1 and Piezo2 channels confers high-strain mechanosensitivity to articular cartilage. Proc Natl Acad Sci U S A 2014;111:E5114–E5122. https://doi.org/10.1073/pnas.1414298111.
3. Servin-Vences RM, Moroni M, Lewin GR, Poole K. Direct measurement of TRPV4 and PIEZO1 activity reveals multiple mechanotransduction pathways in chondrocytes. eLife 2017;6:e21074. https://doi.org/10.7554/eLife.21074.
4. O'Conor CJ, Leddy HA, Benefield HC, Liedtke WB, Guilak F. TRPV4-mediated mechanotransduction regulates the metabolic response of chondrocytes to dynamic loading. Proc Natl Acad Sci U S A 2014;111:1316–1321. https://doi.org/10.1073/pnas.1319569111.
5. Muramatsu S, Wakabayashi M, Ohno T, Amano K, Ooishi R, Sugahara T, Shiojiri S, Tashiro K, Suzuki Y, Nishimura R, et al. Functional gene screening system identified TRPV4 as a regulator of chondrogenic differentiation. J Biol Chem 2007;282:32158–32167. https://doi.org/10.1074/jbc.M706158200.
6. O'Connor CJ, Griffin TM, Liedtke W, Guilak F. Increased susceptibility of Trpv4-deficient mice to obesity and obesity-induced osteoarthritis with very high fat diet. Ann Rheumatic Disease 2013;72:300–304.
7. O'Conor CJ, Ramalingam S, Zelenski NA, Benefield HC, Rigo I, Little D, Wu CL, Chen D, Liedtke W, McNulty AL, et al. Cartilage-specific knockout of the mechanosensory ion channel TRPV4 decreases age-related osteoarthritis. Sci Rep 2016;6:29053.
8. Pingguan-Murphy B, Lee DA, Bader DL, Knight MM. Activation of chondrocytes calcium signalling by dynamic compression is independent of number of cycles. Arch Biochem Biophys 2005;444(1):45–51.
9. Han SK, Wouters W, Clark A, Herzog W. Mechanically induced calcium signaling in chondrocytes in situ. J Orthop Res 2012;30(3):475–481.
10. Braun JH, Gold GE. Diagnosis of osteoarthritis: Imaging. Bone 2012;51(2):278–288. https://doi.org/10.1016/j.bone.2011.11.019.
11. Hayashi D, Roemer FW, Guermazi A. Recent advances in research imaging of osteoarthritis with focus on MRI, ultrasound and hybrid imaging. Clin Exp Rheumatol 2018;36(Suppl. 114:S43–S52.
12. Holmes DF, Kadler KE. The 10_4 microfibril structure of thin cartilage fibrils. Proc Natl Acad Sci U S A 2006;103(46):17249–17254.
13. Moger CJ, Barrett R, Bleuet P, Bradley DA, Ellis RE, Green EM, Knapp KM, Muthuvelu P, Winlove CP. Regional variations of collagen orientation in normal and diseased articular cartilage and subchondral bone determined using small angle X-ray scattering (SAXS). Osteoarthr Cartil 2007;15:682–687.
14. Rittié L. Method for picrosirius red-polarization detection of collagen fibers in tissue sections. In: Rittié L, editor. Fibrosis: Methods and Protocols. Methods in Molecular

Biology. Volume 1627. New York: Humana Press, 2017; p. 395–407. https://doi.org/10.1007/978-1-4939-7113-8_26.

15. Matcher SJ. What can biophotonics tell us about the 3D microstructure of articular cartilage? Quant Imaging Med Surg 2015;5(1):143–158.
16. Ugryumova N, Jacobs J, Bonesi M, Matcher SJ. Novel optical imaging technique to determine the 3-D orientation of collagen fibers in cartilage: Variable-incidence angle polarization-sensitive optical coherence tomography. Osteoarthr Cartil 2009;17:33–42.
17. Shoulders MD, Raines RT. Collagen structure and stability. Annu Rev Biochem 2009;78:929–958.
18. Lakowicz JR. Fluorescence Anisotropy. In: Lakowicz JR, editor. Principles of Fluorescence Spectroscopy. 3rd ed. New York: Springer Science+Business Media, LLC, 2006; p. 353–369.
19. Brasselet S. Polarization-resolved nonlinear microscopy: Application to structural molecular and biological imaging. Adv Optics Photonics 2011;3:205–271.
20. Reiser K, Stoller P, Knoesen A. Three-dimensional geometry of collagenous tissues by second harmonic polarimetry. Sci Rep 2017;7:2642. https://doi.org/10.1038/s41598-017-02326-7.
21. Suzuki M, Mizuno A, Kodaira K, Imai M. Impaired pressure sensation in mice lacking TRPV4. J Biol Chem 2003;278:22664–22668. https://doi.org/10.1074/jbc.M302561200.
22. Preibisch S, Saalfeld S, Tomancak P. Globally optimal stitching of tiled 3D microscopic image acquisitions. Bioinformatics 2009;25:1463–1465.
23. Delignette-Muller ML, Dutang C. Fitdistrplus: An R package for fitting distributions. J Stat Softw 2015;64:1–34. https://doi.org/10.18637/jss.v064.i04.
24. Gusachenko I, Latour G, Schanne-Klein M-C. Polarization-resolved second harmonic microscopy in anisotropic thick tissues. Opt Express 2010;18:19339–19352.
25. Stucky GD, Marder SR, Sohn JE. Linear and nonlinear polarizability: A primer. In: Materials for Nonlinear Optics. Chapter 1, ACS Symposium Series, Vol. 455, March 11, 1991, pp 2–30, doi:https://doi.org/10.1021/bk-1991-0455.ch001.
26. Chen W-L, Li T-H, Su P-J, Chou C-K, Fwu PT, Lin SJ, Kim D, So PTC, Dong C-Y. Second-order susceptibility imaging with polarization-resolved, second harmonic generation microscopy. In Periasamy A, So PTC, König K, editors Multiphoton Microscopy in the Biomedical Sciences X Proc SPIE 2010;7569:1P. https://doi.org/10.1117/12.843015.
27. Clark AL, Votta BJ, Kumar S, Liedtke W, Guilak F. Chondroprotective role of the osmotically sensitive ion channel transient receptor potential vanilloid 4: Age- and sex-dependent progression of osteoarthritis in Trpv4-deficient mice. Arthritis Rheum 2010;62:2973–2983.
28. Lamandé SR, Yuan Y, Gresshoff IL, Rowley L, Belluoccio D, Kaluarachchi K, Little CB, Botzenhart E, Zerres K, Amor DJ, et al. Mutations in TRPV4 cause an inherited arthropathy of hands and feet. Nat Genet 2011;43:1142–1146.
29. Loukin S, Zhou X, Su Z, Saimi Y, Kung C. Wild-type and brachyolmia-causing mutant TRPV4 channels respond directly to stretch force. J Biol Chem 2010;285:27176–22718.
30. Gilchrist CL, Leddy HA, Kaye L, Case ND, Rothenberg KE, Little D, Liedtke W, Hoffman BD, Guilak F. TRPV4-mediated calcium signaling in mesenchymal stem cells regulates aligned collagen matrix formation and vinculin tension. Proc Natl Acad Sci U S A 2019;116:1992–2997.
31. Kiyomatsu H, Oshima Y, Saitou T, Miyazaki T, Hikita A, Miura H, Iimura T, Imamura T. Quantitative SHG imaging in osteoarthritis model mice, implying a diagnostic application. Biomed Optics Express 2015;6(2):405–420. https://doi.org/10.1364/BOE.6.000405.
32. Saitou T, Kiyomatsu H, Imamura T. Quantitative Morphometry for Osteochondral tissues using second harmonic generation microscopy and image texture information. Sci Rep 2018;8:2826. https://doi.org/10.1038/s41598-018-21005-9.
33. Hui Mingalone CK, Liu Z, Hollander JM, Garvey KD, Gibson AL, Banks RE, Zhang M, McAlindon TE, Nielsen HC, Georgakoudi I, et al. Bioluminescence and second harmonic generation imaging reveal dynamic changes in the inflammatory and collagen landscape in early osteoarthritis. Lab Invest 2018;98:656–669.
34. Bergmann T, Maeder U, Fiebich M, Dickob M, Nattkemper TW, Anselmetti D. Categorization of two-photon microscopy images of human cartilage into states of osteoarthritis. Osteoarthr Cartil 2013;21:1074e1082.
35. Kumar R, Grønhaug KM, Romijn EI, Finnøy A, Davies CL, Drogset JO, Lilledahl MB. Polarization second harmonic generation microscopy provides quantitative enhanced molecular specificity for tissue diagnostics. J Biophotonics 2014;8:1–10. https://doi.org/10.1002/jbio.201400086.
36. Mansfield JC, Mandalia V, Toms A, Winlove CP, Brasselet S. Collagen reorganization in cartilage under strain probed by polarization sensitive second harmonic generation microscopy. J R Soc Interface 2018;16:20180611.
37. Gosset M, Berenbaum F, Levy A, Pigenet A, Thirion S, Cavadias S, Jacques C. Mechanical stress and prostaglandin E2 synthesis in cartilage. Biorheology 2008;45(3–4):301–320.
38. Arora PD, Di Gregorio M, He P, McCulloch CA. TRPV4 mediates the Ca^{2+} influx required for the interaction between flightless-1 and non-muscle myosin, and collagen remodelling. J Cell Sci 2017;130:2196–2208. https://doi.org/10.1242/jcs.201665.
39. Servin-Vences MR, Richardson J, Lewin GR, Poole K. Mechanoelectrical transduction in chondrocytes. Clin Exp Pharmacol Physiol 2018;45:481–488.
40. Fox AJS, Bedi A, Rodeo SA. The basic science of articular cartilage structure, composition, and function. Sports Health 2012;4(4):340–351. https://doi.org/10.1177/1941738109350438.
41. Huland DM, Brown CM, Howard SS, Ouzounov DG, Pavlova I, Wang K, Rivera DR, Webb WW, Xu C. In vivo imaging of unstained tissues using long gradient index lens multiphoton endoscopic systems. Biomed Opt Express 2012;3(5):1077–1085. https://doi.org/10.1364/BOE.3.001077.
42. Reismann D, Stefanowski J, Günther R, Rakhymzhan A, Matthys R, Nützi R, Zehentmeier S, Schmidt-Bleek K, Petkau G, Chang HD, et al. Longitudinal intravital imaging of the femoral bone marrow reveals plasticity within marrow vasculature. Nat Commun 2017;8(1):2153. https://doi.org/10.1038/s41467-017-01538-9.
43. Baskey SJ, Andreana M, Lanteigne E, Ridsdale A, Stolow A, Schweitzer ME. Preclinical translation of second harmonic microscopy of meniscal and articular cartilage using a prototype nonlinear microendoscope. IEEE J Transl Eng Health Med 2018;7(1):1800211–1800211. https://doi.org/10.1109/JTEHM.2018.2889496.